Eur Biophys J (2011) 40:503–514
DOI 10.1007/s00249-010-0664-1

ORIGINAL PAPER

Effect of acyl chain structure and bilayer phase state on binding and penetration of a supported lipid bilayer by HPA3

Daniel J. Hirst · Tzong-Hsien Lee · Marcus J. Swann · Sharon Unabia · Yoonkyung Park · Kyung-Soo Hahm · Marie Isabel Aguilar

Received: 25 October 2010 / Accepted: 22 December 2010 / Published online: 11 January 2011

Abstract The effect of acyl chain structure and bilayer phase state on binding and penetration by the peptide HPA3 was studied using dual polarisation interferometry. This peptide is an analogue of Hp(2-20) derived from the N-terminus of *Helicobacter pylori* ribosomal protein L1 (RpL1) which has been shown to have antimicrobial and cell-penetrating properties. The binding of HPA3 to zwitterionic 1,2-dimyristoyl-sn-glycero-3-phosphocholine (DMPC) or 1-palmitoyl-2-oleyl-sn-glycero-3-phosphocholine (POPC) and negatively charged membranes composed of DMPC and 1,2-dimyristoyl-sn-glycero-3-(phosphor-rac-(1-glycerol)) (DMPG) or POPC and 1-palmitoyl-2-oleyl-sn-glycero-3-(phosphor-rac-(1-glycerol)) (POPG) was determined using dual polarisation interferometry (DPI). Mass and birefringence were measured in real time, enabling the creation of birefringence–mass plots for detailed analysis of the changes in lipid bilayer order during the peptide-binding process. HPA3 bound to all four lipids and the binding progressed as a single phase for the saturated gel phase bilayers DMPC and DMPC–DMPG. However, the binding process involved two or more phases, with penetration of the unsaturated fluid phase POPC and POPC–POPG bilayers. Structural changes in the saturated bilayer were partially reversible whereas binding to the unsaturated bilayer resulted in irreversible changes in membrane structure. These results demonstrate that more disordered unsaturated bilayers are more susceptible to further disorganisation and have a lower capacity to recover from peptide-induced structural changes than saturated ordered bilayers. In addition, this study further establishes DPI as powerful tool for analysis of multiphase peptide-insertion processes associated with complex structural changes in the liquid-crystalline membrane.

Keywords Antimicrobial peptide · Hp(2-20) · Dual polarisation interferometry · Supported lipid bilayer · Birefringence

Membrane-active peptides: 455th WE-Heraeus-Seminar and AMP 2010 Workshop.

Electronic supplementary material The online version of this article (doi:10.1007/s00249-010-0664-1) contains supplementary material, which is available to authorized users.

D. J. Hirst · T.-H. Lee · S. Unabia · M. I. Aguilar (✉)
Department of Biochemistry & Molecular Biology, Monash University, Clayton, VIC 3800, Australia
e-mail: mibel.aguilar@med.monash.edu.au

M. J. Swann
Farfield Group, Farfield House, Southmere Court, Electra Way, Crewe Business Park, Crewe CW1 6GU, UK

Y. Park · K.-S. Hahm
Research Center for Proteineous Materials (RCPM), Chosun University, 375 Seosuk-Dong, Dong-Ku, Gwangju, Korea

Introduction

Elucidation of the mechanism by which antimicrobial and cell-penetrating peptides penetrate and disrupt phospholipid bilayers continues to be a significant challenge. This is largely because of the broad range of peptide sequences that have been identified and the apparent differences in membrane-disruption properties (Melo et al. 2009; Shai 2002; Zasloff 2002). In addition, the complexity of the peptide–membrane interaction process requires use of a large number of complementary techniques to explore different aspects of membrane binding (Jin et al. 2003; Mozsolits and Aguilar 2002). In previous studies we demonstrated that dual polarisation interferometry (DPI)

can be used to probe changes in membrane structure in real time during peptide binding (Lee et al. 2010a, b). In particular, we showed that HPA3, a peptide analogue of Hp (2-20) derived from the N-terminus of *Helicobacter pylori* ribosomal protein L1 (RpL1), which has been shown to have antimicrobial and cell penetrating properties, binds to zwitterionic and anionic phospholipid bilayers, but penetrates and causes significantly greater changes in the bilayer structure of negatively charged membrane bilayers (Lee et al. 2010a). Moreover, the extent of DMPC–DMPG bilayer disruption was double that observed for DMPC on binding of HPA3. In addition, the temperature denaturation of DMPC–DMPG was significantly compromised compared with DMPC. These results, which clearly demonstrate that the presence of negatively charged phospholipids enhances the ability of HPA3 to bind and penetrate the membrane, causing significant changes in bilayer structure, are consistent with results previously obtained from fluorescence quenching studies (Lee et al. 2006).

It is well-established that the composition and structure of the lipid bilayer is an important aspect of the internalization mechanisms of antimicrobial and cell-penetrating peptides. A major difference is the distinction between zwitterionic lipids, for example dimyristoylphosphatidylcholine (DMPC) and anionic lipids, for example dimyristoylphosphatidylglycerol (DMPG), both of which are fully saturated with 14 carbon atoms in both acyl chains. However, the degree of saturation of the phospholipid acyl chain plays an important role in bilayer structure and stability. Unsaturated phospholipids, for example palmitoyloleoylphosphatidylcholine (POPC) and palmitoyloleoylphosphatidylcholine (POPG), contain 16 carbon atoms in the saturated palmitoyl acyl chain at glycerol C1 and 18 carbon atoms in the monounsaturated oleyl chain at glycerol C2. We have previously investigated the importance of lipid unsaturation in the membrane interaction of HPA3 (Mereuta et al. 2009). The results demonstrated the extent to which the greater unsaturation present in 1,2-dioleoyl-sn-glycero-3-phosphocholine (DOPC) acyl chains compared with POPC, leads to an enhancement of the penetration of HPA3 into planar lipids made of DOPC lipids, and mediated transmembrane translocation.

In this study we have investigated the ability of HPA3 to cause significant alterations in membrane geometry, and lipid packing and ordering in model membranes composed of the unsaturated POPC and POPG using DPI (Lee et al. 2010a, b; Mashaghi et al. 2008; Popplewell et al. 2007; Yu et al. 2009). DPI is waveguide technology which has been used to study peptide–membrane interactions by depositing a lipid bilayer on the planar solid surface and then injecting peptides on to the lipid bilayer (Swann et al. 2004). DPI has advantages over other optical biosensor techniques (Hall et al. 2003; Mozsolits and Aguilar 2002) because of its simultaneous real-time measurement of membrane refractive index, thickness, mass, and density (Lee et al. 2010a, b; Yu et al. 2009). Birefringence is a measure of the order in the system; high birefringence indicates a well ordered system whereas low birefringence indicates a more disordered system. Thus, by measuring birefringence it is possible to detect and track changes in the structure of the supported lipid bilayer, leading to greater understanding of the effect of the binding of biomolecules to biological membranes. The objective of this study was to characterise the binding of HPA3 by monitoring changes in membrane properties such as mass, thickness, and birefringence, and to provide greater insight into the membrane dynamics associated with peptide penetration, because of its ability to sensitively detect changes in lipid membrane structure and distribution.

Materials and methods

Chemicals and reagents

1,2-Dimyristoyl-sn-glycero-3-phosphocholine (DMPC), 1,2-dimyristoyl-sn-glycero-3-(phosphor-rac-(1-glycerol)) sodium salt (DMPG), 1-palmitolyl-2-oleyl-sn-glycero-3-phosphocholine (POPC), and 1-palmitolyl-2-oleyl-sn-glycero-3-(phosphor-rac-(1-glycerol)) (POPG) were purchased from Avanti Polar Lipids (Alabaster, AL, USA). 4-Morpholinepropanesulfonic acid (MOPS), sodium dodecyl sulfate (SDS), calcium chloride, and sodium chloride, all analytical-grade, were purchased from Sigma–Aldrich (St Louis, MI, USA). Chloroform, methanol, and ethanol, all HPLC-grade, were purchased from Merck (Darmstadt, Germany). Hellmanex II was purchased from Hellma (Müllheim, Germany). Water was quartz-distilled and deionised using a Milli-Q system equipped with UV oxidation to remove organic residues (Millipore, Bedford, MA, USA). HPA3 (AKKVFKRLEKLFSKIWNWK) was synthesised by solid-phase methods, purified to >98% purity by reversed-phase high-performance liquid chromatography, and characterised by amino acid composition analysis and matrix-assisted laser desorption ionisation (MALDI) mass spectrometry as previously described (Lee et al. 2010a).

Preparation of liposomes

Stock solutions of 2 mM DMPC, DMPG (in 3:1 chloroform–methanol), POPC, and POPG in chloroform were prepared; after setting aside sufficient DMPC and POPC these were then mixed to form DMPC–DMPG and POPC–POPG solutions with a molar ratio of 4:1 in both cases.

Aliquots containing 0.8 μmol of each lipid mixture used (DMPC, DMPC–DMPG, POPC, POPC–POPG) were dried by use of a gentle stream of N_2 gas in a Pyrex test tube, and vacuum dried overnight to form lipid films. These were then hydrated with 10 mM MOPS buffer, 150 mM NaCl, pH 7 buffer at 37°C in a shaker–incubator for 1 h; the samples were then ultrasonicated in a bath-type sonicator for 30 min, generally resulting in a clear solution. This solution was extruded 21 times through a 50-nm polycarbonate membrane, by means of an Avestin Liposofast extruder (Avestin, ON, Canada).

Dual polarisation interferometry

The *Ana*light Bio200 containing a silicon oxynitride FB80 AnaChip was used to perform all dual polarisation interferometry measurements. An independent Harvard Apparatus PHD2000 programmable syringe pump was used to control the flow rate of bulk buffer. The bulk buffer was 10 mM MOPS, 150 μM NaCl, pH 7 for all experiments. The chip was cleaned at 28°C with 10% Hellmanex II, 2% SDS and absolute ethanol, as previously described (Lee et al. 2010a). The optical properties of the chip were then calibrated at 20°C using 80% (*w*/*w*) ethanol and water, followed by calibrations of the bulk buffer at 20°C and 28°C. The final liposome solution (200 μL) was then injected at 20 μL/min, forming a stable bilayer at 28°C in the presence of 1 mM $CaCl_2$. The divalent cation Ca^{2+} is important in the formation of the bilayer via direct liposome adsorption on a planar solid support. Addition of $CaCl_2$ is required to ensure reproducible deposition of the liposomes and formation of the phospholipid bilayer. The absence of Ca^{2+} results in the formation of inconsistent geometric structures and liposomes. The concentration of Ca^{2+} is lipid composition and concentration-dependent and also varies with types of substrate. (Benes et al. 2004; Mashaghi et al. 2008).

The bilayer was then left to stabilise for 30 min before being cooled to 20°C. When the signal from the chip had stabilised, 160 μL of a peptide solution was injected at 40 μL/min in order to observe binding events. HPA3 was dissolved in bulk buffer and injected at concentrations of 2, 5, 10, 20, and 40 μM on to each bilayer type in successive experiments with the surface being cleaned with Hellmanex II, 2% SDS and ethanol and a new bilayer formed between experiments. Consecutive injections were also performed on a single bilayer for each lipid type using the same concentrations as for the single peptide injections just described; the lowest concentration (usually 2 μM) was injected and left for 30 min to equilibrate before the next highest concentration (usually 5 μM) was injected, and all the other peptide concentrations were then introduced sequentially with a 30 min waiting time after each injection.

Calculation of mass per unit area for an adsorbed layer

Two orthogonal polarizations are passed through the sensor chip creating two different waveguide modes, namely transverse electric (TE) and transverse magnetic (TM) waveguide modes. Each mode generates an evanescent field from the top sensing waveguide surface interacting with materials coming into contact with the sensor surface and resulting in a change in RI. Thus, birefringence can be obtained with DPI by calculating the difference between two effective refractive indices, namely RI of transverse magnetic (TM) waveguide mode (nTM) and RI of transverse electric (TE) waveguide mode (nTE).

The mass per unit area for an adsorbed anisotropic layer is calculated using the de Feijter formula (de Feijter et al. 1978), for m_{lipid} the mass of lipid in the bilayer and m_{peptide} the mass of peptide bound to the bilayer:

$$m_{\text{lipid}} = d_f(n_{\text{iso}} - n_{\text{buffer}})/(dn/dc)_{\text{lipid}} \quad (1)$$

$$m_{\text{peptide}} = d_f(n_{\text{iso}} - n_{\text{buffer}})/(dn/dc)_{\text{peptide}} \quad (2)$$

where d_f is the thickness of the bilayer, n_{iso} is the average refractive index of the bilayer calculated from the experimentally obtained refractive index values n_{TM} and n_{TE} using the formula:

$$n_{\text{iso}} = \sqrt{(n_{\text{TM}}^2 + 2n_{\text{TE}}^2)/3} \quad (3)$$

n_{buffer} is the refractive index of the buffer, experimentally determined to be 1.3349 at 20°C, and $(dn/dc)_{\text{lipid}}$ and $(dn/dc)_{\text{peptide}}$ are the refractive index increments of the lipid and peptide, using values of 0.135 and 0.185 mL/g for lipids and peptides, respectively (de Feijter et al. 1978; Mashaghi et al. 2008).

Calculation of birefringence for an adsorbed layer

If the thickness of a bilayer is known the birefringence value can be calculated (Horvath and Ramsden 2007; Lee et al. 2010a) from the difference between n_{TM} and n_{TE}. Changes in the thickness of the layer are determined by fixing the refractive index of the bilayer at an assumed value of 1.47. Mass and birefringence data were derived using the Analight® Explorer program as previously described (Lee et al. 2010a). The deposition of the bilayers was monitored by the rate of TM and TE phase changes versus changes in mass together with the evolution of birefringence, as shown in the Supplementary data for DMPC. The change in birefringence as

a function of mass of peptide bound was then used to characterise the effect of peptide binding on membrane structure. DPI measures the lipid and peptide mass per unit area (unaffected by surrounding buffer) at very high sensitivity and is also sensitive to the effect of alignment of the lipid (birefringence). The output can be compared with data obtained by use of other techniques, for example quartz-crystal microbalance with dissipation (QCM-D), which derives a mass per unit area that includes the associated buffer and dissipation that relates to the rigidity of the layer. Indeed the different information provided by the two techniques has already been correlated by others (Zwang et al. 2010) to provide a greater level of insight into the structure of a supported lipid bilayer. Overall, therefore, we have used the thickness and birefringence to define the quality of our deposited membrane. We then focussed on changes in birefringence during peptide binding because this can reveal more details about the effect of the peptide on the membrane structure than a change in thickness, and potentially allow a mechanism of action to be defined.

Circular dichroism spectroscopy

CD experiments were performed using a Jasco (MD, USA) 815 spectropolarimeter using a 0.1 cm path length quartz cell. All spectra were obtained at 20°C. DMPC, DMPC–DMPG (4:1), POPC, and POPC–POPG (4:1) small unilamellar vesicles were prepared by hydrating in 10 mM sodium phosphate buffer, pH 7.4, and were extruded through a polycarbonate filter (100 nm pore diameter). HPA3 (1 mM in sodium phosphate buffer) was then added to the liposome solution at a final peptide concentration of 20 μM, resulting in a peptide-to-lipid molar ratio of 1:50. The peptide–liposome solution was mixed by inversion and incubated for 2 min. Each spectrum was obtained by averaging five scans in the 190–260 nm wavelength range. All CD spectra are reported as mean residue ellipticity $[\theta]$ in deg cm^2 dmol^{-1}. In all measurements CD spectra of the same buffer and/or liposome solutions without peptides were applied as baseline. The alpha-helical content was measured by use of the formula:

$$\%[\alpha] = \frac{[\theta]_{222}}{\left[[\theta]_{\text{helix}} \times (1 - 2.57/n)\right]} \times 100$$

where $[\theta]_{\text{helix}}$ is the ellipticity of a peptide with 100% helical content of infinite length, with a value of −39,500 deg cm^2 dmol^{-1}, $[\theta]_{222}$ is the ellipticity of the solution at 222 nm, and n is the number of residues of the peptide (Chen et al. 1974; Lee et al. 2010a).

Results

Formation of stable lipid bilayers

Before the binding properties and effects of peptides on the membrane can be observed it is essential that a stable, reproducible and well defined bilayer structure is produced. Formation of the lipid bilayer in situ occurs at 28°C and with a concentration of 1 mM $CaCl_2$ in order to maintain the stability and uniformity of the membrane (See supplementary data). Measurement of the lipid bilayer after cooling to 20°C showed that results were consistent and reproducible, as shown in Table 1. Values obtained for DMPC and DMPC–DMPG are similar to those previously obtained (Lee et al. 2010a). The clearest distinction between the bilayer types is the difference in birefringence between the saturated lipid bilayers (0.0222 and 0.0229) and the unsaturated lipid bilayers (0.185 and 0.0177). This difference is present despite the general similarity in the other properties of the bilayer between the different bilayer types. This suggests that the presence of the unsaturated bond in POPC and POPG acts to cause greater disorder in the bilayer, perhaps because of less efficient packing of lipid molecules.

General features of peptide binding events

Peptide solutions were injected into the *Ana*light Bio200 DPI for 4 min; plots of mass against time for each lipid mixture are shown in Figs. 1a, b, 2a, b. During this period the peptide binds to the bilayer surface, generally characterised by a rapid increase in the mass on the surface, followed by a more gradual increase as remaining binding sites on the bilayer are taken up by the peptide. After 4 min, the flow of buffer is restored, resulting in the dissociation phase in which a proportion of the bound peptide dissociates and leaves the bilayer surface until equilibrium is reached. This period is usually identified by a drop in the mass. In addition, peptides that are bound to the membrane may also penetrate it, moving further into the hydrophobic region of the bilayer.

Single injections of HPA3 on to DMPC and DMPC–DMPG

The changes in mass and birefringence for the binding of HPA3 to DMPC and DMPG were calculated for the association and dissociation phases; the resulting plots are shown in Fig. 1. It is evident from the mass vs. time plots that HPA3 (Fig. 1a) binds strongly to DMPC, with a mass change of as much as 0.9 ng/mm^2 observed at 20 μM. The binding was also concentration-dependent from 2 to 10 μM, but did not

Table 1 Properties of supported lipid bilayers as observed by use of dual polarization interferometry techniques at 20°C

Lipid	RI	Density (g/cm^3)	Thickness (nm)	Mass (ng/mm^2)	Birefringence	Area per molecule (Å^2)
DMPC	1.470 ± 0.004	1.00 ± 0.03	4.65 ± 0.13	4.68 ± 0.12	0.0221 ± 0.0006	48.1
DMPC–DMPG 4:1	1.470 ± 0.002	1.01 ± 0.03	4.60 ± 0.08	4.64 ± 0.08	0.0229 ± 0.0003	48.7
POPC	1.471 ± 0.004	1.01 ± 0.03	4.87 ± 0.15	4.71 ± 0.15	0.0185 ± 0.0007	53.6
POPC–POPG 4:1	1.470 ± 0.001	1.00 ± 0.01	4.54 ± 0.04	4.56 ± 0.05	0.0177 ± 0.0011	55.5

Values are means from 20 observations; the error is given as one standard deviation from the mean

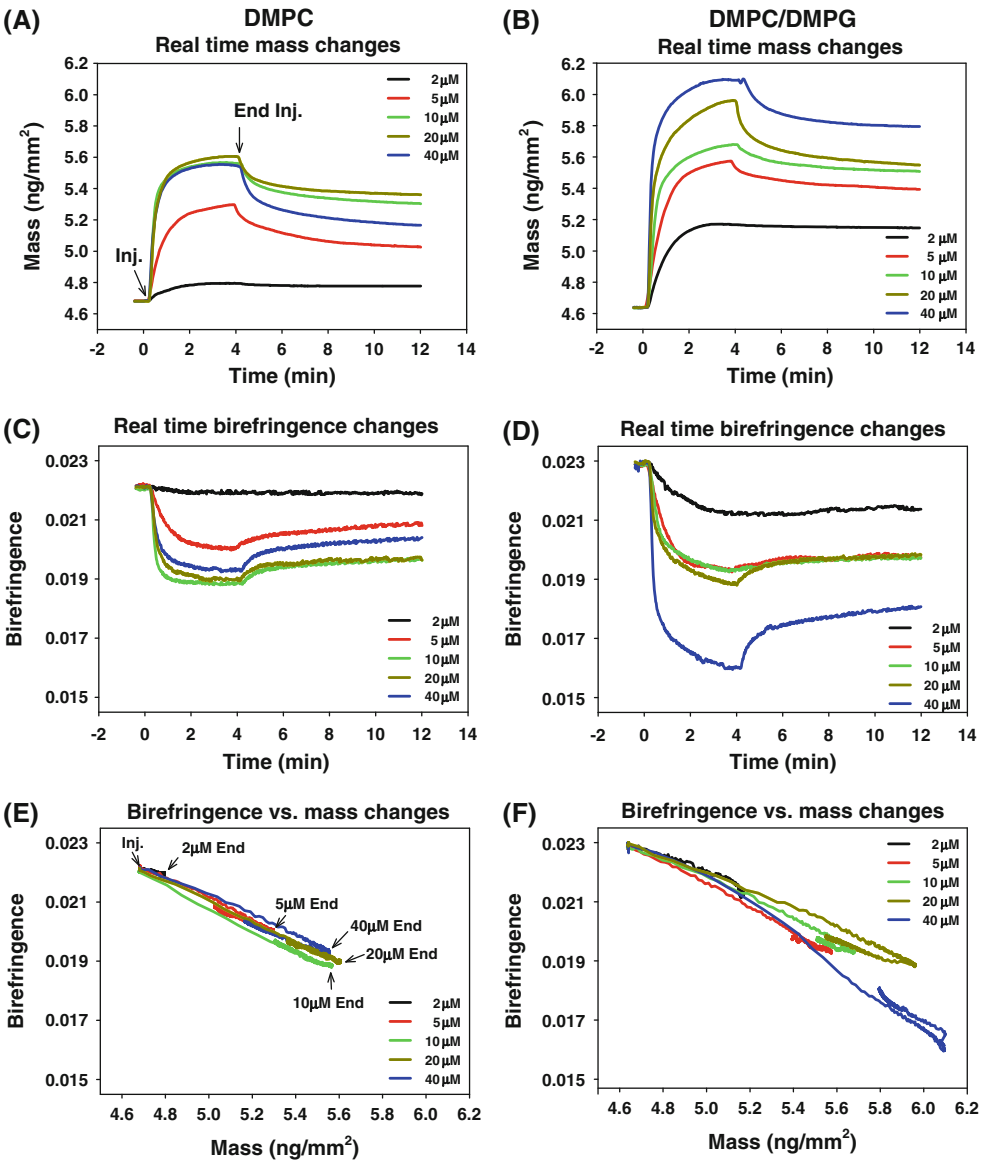

Fig. 1 Measurements of bilayer mass and birefringence versus time during single injections of HPA3 on to DMPC and DMPC–DMPG. Plots of mass vs. time for single injections of HPA3 on to **a** DMPC and **b** DMPC–DMPG; birefringence vs. time for single injections of HPA3 on to **c** DMPC and **d** DMPC–DMPG; birefringence vs. mass plots for single injections of HPA3 on to **e** DMPC and **f** DMPC–DMPG. Peptide was injected at time = 0 min corresponding to the association phase; after 4 min, the peptide solution was replaced by buffer corresponding to the dissociation phase. For the plots of birefringence vs mass, the end of injection corresponds to the change in direction of each line. Peptide concentrations ranged from 2 to 40 μM

increase significantly thereafter, indicating that the membrane had become saturated with peptide. Interestingly, the 40 μM concentration shows similar binding to the 10 and 20 μM concentrations but with greater dissociation (loss of mass). Overall it is not possible to determine affinities by plotting amount of peptide bound versus peptide concentration, because these plots only yield the affinity of peptides for the membrane if there is a simple 1:1 binding mechanism. However, as this and many other studies (Gehman et al. 2008; Mozsolits et al. 2001; Papo and Shai 2003) have shown, peptide binding to membranes consists of several steps and even relative affinity was not determined.

However, the mass vs. birefringence plots (Fig. 1e) enable features of the binding mechanism to be discerned

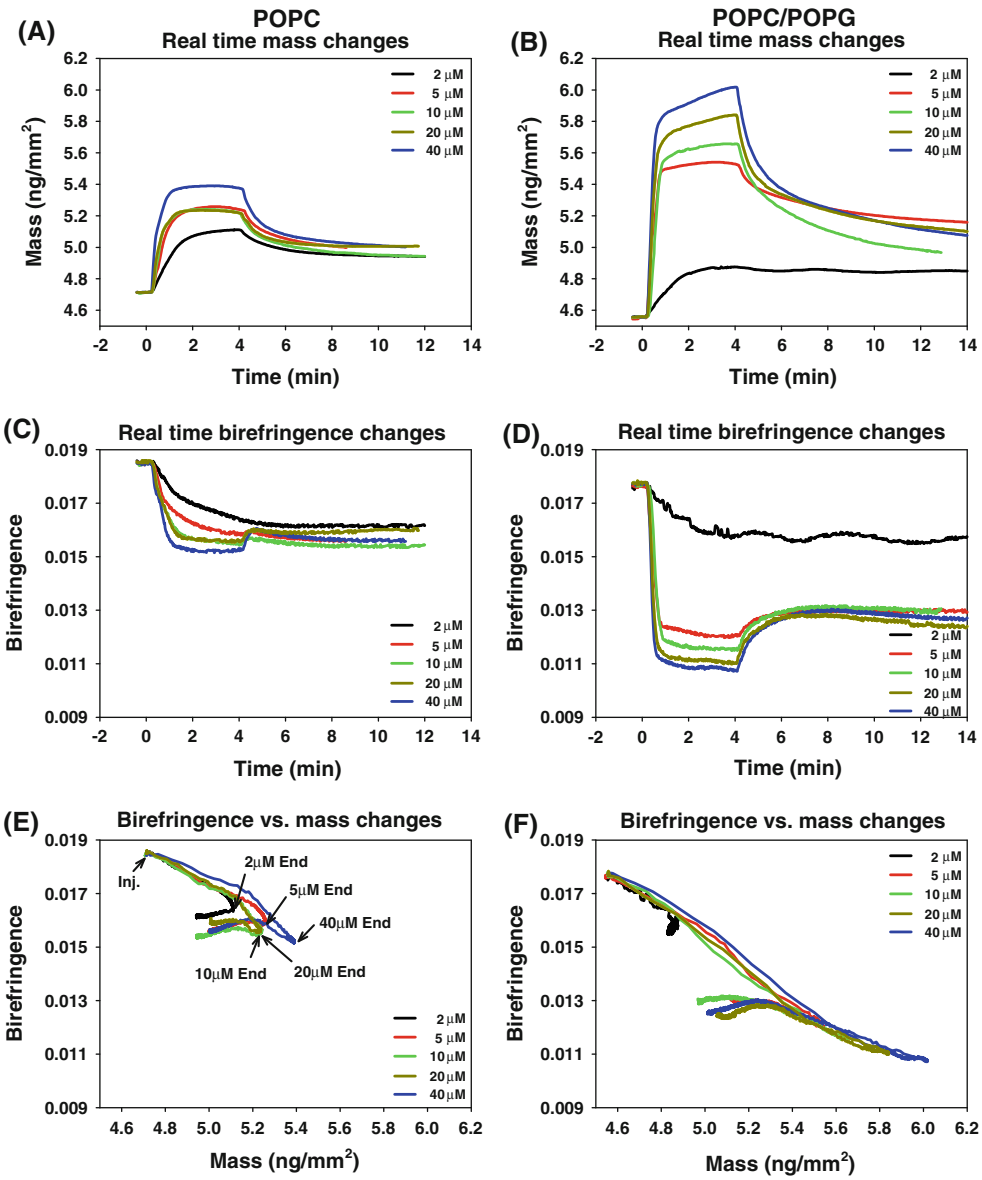

Fig. 2 Measurements of bilayer mass and birefringence over time during single injections of HPA3 on to POPC and POPC–POPG. Plots of mass vs. time for single injections of HPA3 on to **a** POPC and **b** POPC–POPG; birefringence vs. time for single injections of HPA3 on to **c** POPC and **d** POPC–POPG; birefringence vs. mass plots for single injections of HPA3 on to **e** POPC and **f** POPC–POPG. For the plots of mass vs. time, peptide was injected at time = 0 min corresponding to the association phase; after 4 min, the peptide solution was replaced by buffer corresponding to the dissociation phase. For the plots of birefringence vs mass, the end of injection corresponds to the change in direction of each line. Peptide concentrations ranged from 2 to 40 μM

that cannot be readily identified from plots of either mass or birefringence against time. The plots are presented as a line tracking the state of the bilayer across the time period of the experiment, starting at the top left corner before binding of the peptide, progressing to the bottom right (indicating higher mass/lower birefringence) during the binding phase and then partially returning as the peptide dissociates after the injection is completed. It is evident from Fig. 1e that HPA3 binding causes a simple linear decrease in DMPC birefringence, which is followed by a dissociation phase that essentially reverses part of the structural changes that occurred during binding, indicated by the plot reversing back along the trajectory of the association phase. This type of binding–dissociation pattern indicates that the binding of the peptide causes a significant drop in birefringence but has no permanent effect on the structure of the membrane, suggesting that in this case the peptide is only binding near the surface, and is not actually fully penetrating the membrane.

DMPC and DMPG differ structurally in that DMPG is anionic whereas DMPC is zwitterionic. Because HPA3 is strongly cationic with a net charge of +6, significant differences would be expected between its binding to DMPC–DMPG compared with DMPC alone. Indeed, as can be seen in Fig. 1b, HPA3 binds more to DMPC–DMPG, with a mass change of 1.5 ng/mm^2. The changes in birefringence over time (Fig. 1d) for HPA3 are also higher for DMPC–DMPG than for DMPC, indicating a greater degree of disruption of the negatively charged membrane bilayer. This effect is further evident in the plot of birefringence

versus mass in Fig. 1f, which shows a series of downward sloping parallel lines for the full range of peptide concentrations.

Single injections of HPA3 on to POPC and POPC–POPG

POPC contains a double bond in one of its chains, causing the bilayer to adopt the liquid phase (as opposed to the gel phase in DMPC) and lowering the birefringence but with little change in the thickness compared with DMPC (Table 1). The mass and birefringence data for the binding of HPA3 to POPC and POPC–POPG are plotted in Fig. 2. The mass change for HPA3 on POPC (Fig. 2a) is slightly less than that for DMPC, with a maximum mass change of 0.7 ng/mm^2 compared with 0.9 ng/mm^2 for DMPC. Notably, however, the mass change for the lowest concentration (2 μM) on POPC is approximately 0.4 ng/mm^2, much higher than for DMPC where it was 0.1 ng/mm^2 reflecting a different concentration threshold for binding and penetration.

Overall, the plot of birefringence against time for HPA3 on POPC (Fig. 2c) has two significant features associated with the dissociation phase. First, at 2 μM peptide, there is no recovery in the birefringence during the dissociation phase, despite a significant decrease in mass. Such a pattern was not observed with either DMPC or DMPC–DMPG, suggesting that the mechanism involved in the binding differs between the two types of lipids. Second, at the higher HPA3 concentrations, there is some recovery in the birefringence, with each successive concentration showing a higher short-term increase in the birefringence. Finally, it can also be seen that even after the dissociation phase, there continues to be a slow *decrease* in birefringence until about 8 min after the initial injection, indicating further disordering caused by the bound peptide.

The plot of birefringence versus mass for HPA3 on POPC (Fig. 2e) shows a clearly different pattern to that observed for the DMPC. The binding process consists of at least two distinct phases: an initial binding phase characterised by increasing mass and decreasing birefringence, and a second binding phase characterised by a further increase in mass and loss in birefringence but with a steeper gradient. The second phase begins at the time point at which the birefringence reaches about 0.0167 and the mass reached about 5.2 ng/mm^2. The dissociation then occurs, and (except for 2 μM HPA3), is characterised by decreasing mass and increasing birefringence at the same gradient as the first binding process—suggesting the dissociation is a partial reversal of the first binding process. Finally there is an equilibration phase in which the mass decreases further, and the birefringence drops slightly, as observed earlier for the graphs vs. time.

The mass vs. time plots (Fig. 2b) show significant binding of HPA3 to POPC–POPG with a mass change of up to 1.5 ng/mm^2, which is similar to the results seen for DMPC–DMPG. The birefringence–time plots (Fig. 2d) for HPA3 on POPC–POPG are similar in the dissociation phase to POPC, in that the recovery of the birefringence consistently increases from almost nothing for the lowest concentration (2 μM) to a very sharp recovery for the highest concentration (40 μM). The birefringence–mass plot (Fig. 2f) for POPC–POPG has a somewhat different pattern from that seen for POPC—here, instead of two clearly different binding phases, there are three segments of which the second has a steeper gradient than the others. There does not seem to be any consistent point at which the second phase begins and concludes, starting anywhere between 4.9 and 5.3 ng/mm^2 for mass and between 0.015 and 0.0165 for birefringence (although it should be noted that the binding here was very rapid). The dissociation initially retraces the final phase of the binding and then to the left, suggesting further birefringence is being lost relative to the same mass level during the binding phase.

Consecutive injections of HPA3 on to POPC and POPC–POPG

In the previous sections each injection was performed with a fresh bilayer which enables the effect of individual concentrations to be evaluated. However, it is possible to observe how binding proceeds when peptides are injected on to an already bound bilayer by using consecutive injections (Lee et al. 2010a). The consecutive binding of HPA3 to POPC is shown in Fig. 3a where the mass bound with each consecutive injection increased to a maximum mass change of approximately 0.5 ng/mm^2. This level of binding is similar to the values seen for single injections of this peptide–lipid combination. The maximum mass change increased significantly for 2 μM and 5 μM injections but there were only small increases with further injections. Moreover, the level of dissociation was greater at higher concentrations than for 2 μM. A similar pattern is seen for birefringence; there seems to be very little recovery of the birefringence for lower concentrations, and none at 2 μM with the birefringence continuing to drop after the injection finishes. The mass-birefringence plot (Fig. 3c) reveals some important features of the binding process. For the 2 μM concentration there are two phases: a binding phase followed by a dissociation phase in which the concentration continues to drop. This is similar to the pattern observed with the 2 μM single injection (with the same method up to this point). When 5 μM peptide is then injected, the two binding phases observed above can be seen along with the normal dissociation phase (decreased mass and increased birefringence) but no evidence of a

further equilibration phase with loss of mass and stable or dropping birefringence. After this point the shape for consecutive injections is very different from that for the single injections, behaving similarly to the DMPC experiments with just a single binding phase, and a dissociation phase that partially retraces the binding phase.

The injection of HPA3 on to POPC–POPG results in strong binding to the bilayer of about 1.2 ng/mm^2, slightly less than that seen for single injections, as shown in Fig. 3b. The consecutive injections also show the mass increasing significantly further at the higher concentrations; here the 40 μM maximum mass bound was approximately 30% higher than the 10 μM maximum mass bound. There was little mass loss during the dissociation phase for the 2 μM concentration of HPA3, but for higher concentrations substantial mass loss was observed, suggesting that much of the additional binding at higher concentrations is largely surface binding. The birefringence also drops substantially; similar to the measurements of mass, there is no recovery after the 2 μM injection but there was a recovery in the birefringence after the injections at higher concentrations. The birefringence–mass plot (Fig. 3d) charts show patterns related to those seen in the single injections (Fig. 1f). For 2 μM, binding (black curve) was characterised by increasing mass and decreasing birefringence, followed by slightly decreasing mass and a continuing decrease in birefringence. For 5 μM HPA3 (red curve) there is a distinct pattern that is very similar to that seen in the single injections—a binding curve composed of three segments, the second of which has a steeper mass–birefringence gradient than the other. This suggests a significant structural change in the bilayer at this point; it begins at a mass value of 5.1 ng/mm^2, which is similar to that seen for the altered binding slope for HPA3 on POPC. The dissociation curve then has decreased mass and increased birefringence, and initially follows the binding curve before moving away with lower birefringence. The final three concentrations give linear plots consistent with surface binding, indicating that the complex membrane structure changes occurring at the lower concentrations are

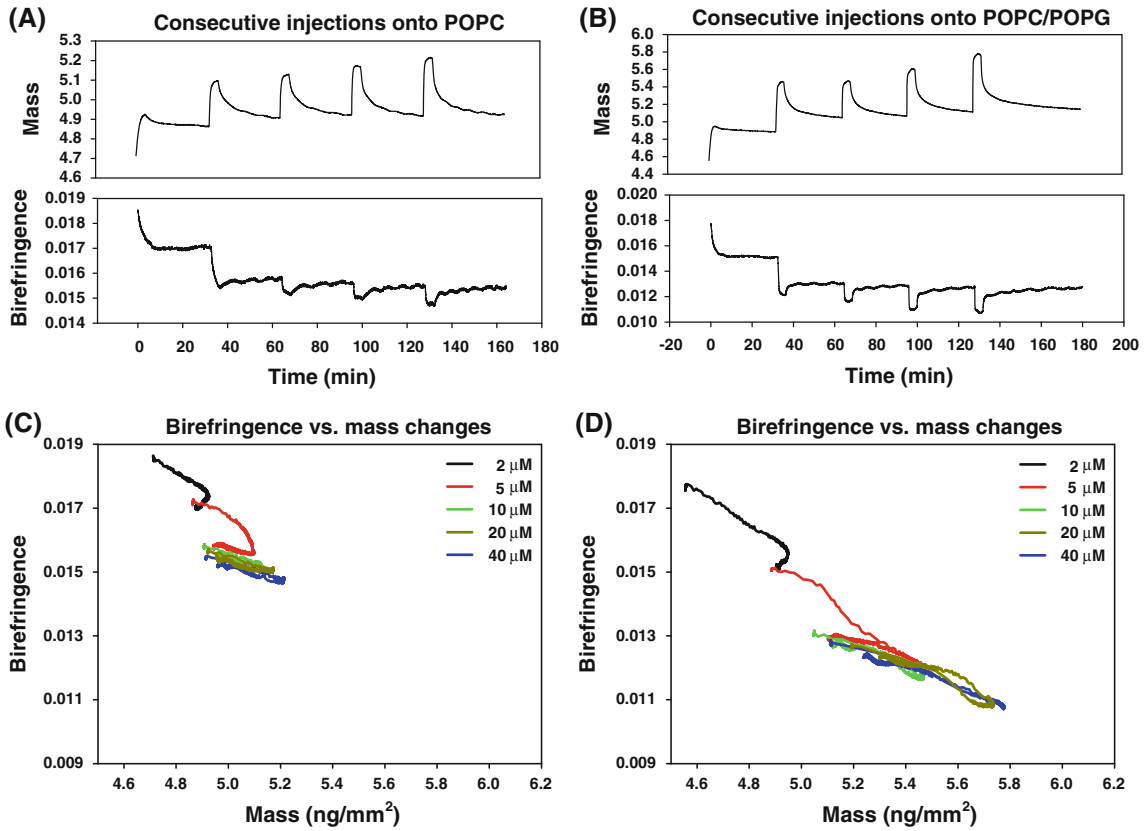

Fig. 3 Measurements of bilayer mass and birefringence over time during consecutive injections of HPA3 on to POPC and POPC–POPG. Plots of mass and birefringence over time for consecutive injections of HPA3 on to **a** POPC and **b** POPC–POPG. Peptide was injected at time = 0 min corresponding to the association phase; after 4 min, the peptide solution was replaced by buffer corresponding to the dissociation phase. Consecutive injections were made every 32 min; concentrations were 2, 5, 10, 20, and 40 μM from *left* to *right*. Plots of birefringence versus mass for binding of HPA3 on to **c** POPC and **d** POPC–POPG respectively—the end of injection corresponds to the change in direction of each *line*. Note shifted *y*-axis scale for **d**

complete and there is very little subsequent permanent binding.

Circular dichroism spectroscopy

Circular dichroism spectra were obtained in buffer alone and with a peptide-to-lipid ratio of 1:50. HPA3 resulted in a single minimum at approximately 198 nm in buffer solution and a similar pattern in DMPC (Fig. 4), indicative of a random coil structure. In the presence of DMPC–DMPG and POPC–POPG the spectrum contained a maximum at 195 nm and a double minimum at 210 and 220 nm, indicating that the peptide has adopted an alpha-helical conformation. The results for POPC did not closely follow any normally observed pattern, with a single minimum at 195 nm and the spectrum returning to zero at 250 nm. There was no significant helical content for HPA3 in phosphate buffer and DMPC (2.2% in buffer and 3.9% for DMPC). However, there was significant helical structure in DMPC–DMPG (13.7%), POPC (9.0%), and POPC–POPG (10.4%) although the figure for POPC should be viewed with caution because of the unusual shape of the spectrum. Previous research had found the helical content of HPA3 on DMPC–DMPG to be 26.2% for the same conditions (Lee et al. 2010a).

Discussion

It has been previously shown that HPA3 causes significant disruption to membrane bilayer structure (Lee et al. 2010a; Mereuta et al. 2009) and to unravel the molecular mechanism of action, it is important to characterise the modulating effects on the membrane structure throughout the process of peptide binding leading to penetration. In this study, DPI has been used for detailed comparative analysis of HPA3 binding to saturated and unsaturated lipid bilayers and, particularly, between the membrane gel and liquid-crystalline states. Specifically, the overall process of HPA3-induced changes in membrane structure was analysed by the real-time changes in bound peptide mass as a function of bilayer birefringence. Overall, the results obtained show significant differences in binding properties and changes in membrane structure during this binding, particularly between the zwitterionic bilayers (DMPC and POPC) and the anionic bilayers (DMPC–DMPG and POPC–POPG). HPA3 bound well to all bilayers (Tables 1, 2), binding more to the anionic lipid bilayers DMPC–DMPG and POPC–POPG, than to the zwitterionic lipids DMPC and POPC. Because HPA3 is highly positively charged (+6), it would be expected to bind more strongly to the anionic lipids than to the zwitterionic lipids because of electrostatic forces. However, the significant binding to DMPC and POPC demonstrates that HPA3 binding is not solely governed by positive charge.

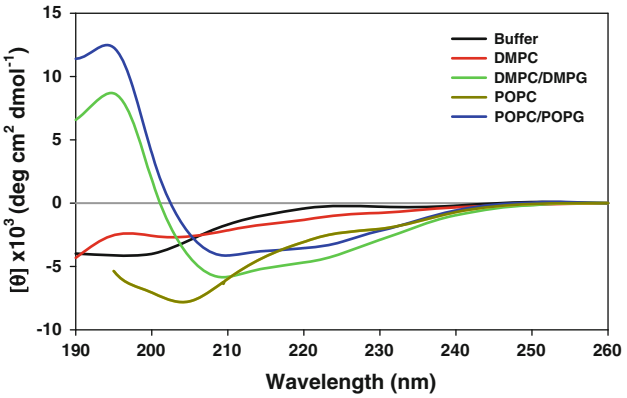

Fig. 4 CD spectra of peptide–lipid solutions: 20 μM HPA3 in 10 mM MOPS buffer, pH 7 (*black line*), and in 1 mM DMPC (*red line*), 1 mM DMPC–DMPG (*green line*), 1 mM POPC (*light brown line*), and 1 mM POPC–POPG (*blue line*) liposomes

The delineation of the interaction mechanisms of peptides with membranes involves understanding the binding characteristics, for example kinetics and affinity, together with the changes in membrane structure associated with the binding process. Mass-birefringence plots, which reveal the changes in membrane ordering that occur during peptide binding, enable very detailed and subtle differences in the interactions between lipids and peptides to be visualised. For example, while the real time changes in mass and birefringence for HPA3 binding to DMPC (Fig. 1a, c) and POPC (Fig. 2a, c) are quite similar, as are the plots for DMPC–DMPG and POPC–POPG (Figs. 1b, d, 2b, d), closer inspection reveals a difference in the dissociation pattern. These subtle differences in binding properties can be further investigated by analysis of the plots of birefringence vs. mass (Fig. 1e, f, 2e, f) which clearly show the different effects of HPA3 binding to the four different bilayers.

The plots obtained in these experiments can be separated into two categories: those on saturated lipids (DMPC and DMPC–DMPG) and those on unsaturated lipids (POPC and POPC–POPG). The unsaturated lipids have a double bond in one of the two acyl chains that introduces a bend in the molecule resulting in different physical properties. In particular the two lipid types have different phase transition temperatures for the gel–fluid transition; for the saturated lipids the transition is at 23°C whereas for unsaturated lipids it is at −2°C. Therefore, in these experiments (conducted at 20°C) the saturated bilayers are in the gel phase and the unsaturated bilayers are in the fluid phase; as a result the effect of the bilayer phase on peptide binding shows clear differences. These differences can be clearly

Table 2 Summary of changes to membrane properties resulting from peptide binding

Bilayer	Maximum mass change (ng/mm^2)	Maximum birefringence change	Equilibrium mass change (ng/mm^2)	Equilibrium birefringence change
Single injections				
DMPC	0.9256	−0.0033	0.6692	−0.0024
DMPC–DMPG	1.4575	−0.0070	1.1514	−0.0047
POPC	0.6770	−0.0033	0.2938	−0.0029
POPC–POPG	1.4613	−0.0070	0.5620	−0.0052
Consecutive injections				
POPC	0.5026	−0.0038	0.2118	−0.0030
POPC–POPG	1.2226	−0.0070	0.5871	−0.0052

Maximum mass and birefringence change refers to the greatest difference in those properties between the bilayer before injection and any stage of binding. Equilibrium mass and birefringence change refers to the greatest difference observed in those properties once the bilayer has been allowed to reach equilibrium following binding

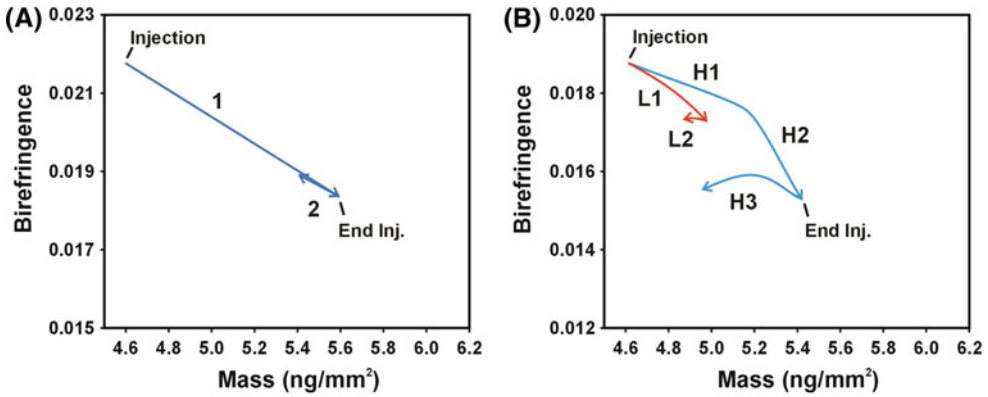

Fig. 5 Generalised birefringence-mass plots showing general profiles in the bilayer properties for HPA3 binding and dissociation. **a** Profile for binding to the saturated lipids DMPC and DMPC–DMPG, with the binding phase 1 and dissociation phase 2 labelled. **b** Profiles for binding to the unsaturated lipids POPC and POPC–POPG for low and high concentrations. Binding phase L1 and dissociation phase L2 labelled for low concentrations, binding phases H1 and H2 and dissociation phase H3 labelled for high concentrations

seen in Fig. 5, a simplified representation of the mass-birefringence plots seen in the Results section for which significant binding was observed.

The birefringence–mass plot for saturated lipids (Fig. 5a) is relatively simple, with a linear binding phase **1** tracing from the top left to the bottom right, with increased mass and decreased birefringence. This reflects the binding of the peptide to the bilayer (increased mass), with partial penetration into the hydrophobic interior causing disruption of the lipid packing and loss of birefringence. This is followed by a dissociation phase **2** which partially retraces the original binding phase and represents the loss of peptide that is washed off when the injection is complete, while the rest of the peptide remains bound to, possibly penetrating, the bilayer.

For unsaturated lipids the birefringence-mass plot (Fig. 5b) is more complex. There are two different possibilities here—one at high concentration and one at low concentration. At low concentrations the binding phase **L1** is almost linear; however, the dissociation phase **L2** does not retrace the binding phase, instead tracing to the left after the injection is complete. This shows that although some peptide may be lost during dissociation at low concentrations, the bilayer experiences irreversible changes in its packing that mean it is no longer able to recover its initial structure.

For higher concentrations the binding phase is split into two parts: **H1**, with a relatively shallow gradient, and **H2**, with a steeper gradient. At first, binding proceeds similarly to that on the saturated bilayers, but once it reaches a critical threshold the gradient changes, representing the structural reorganisation of the bilayer as additional peptide binds. Once the binding phase is complete, the dissociation phase **H3** ensues, in which the plot traces towards the top left before turning to the left. As for phase **L2** this represents the loss of mass from the bilayer surface without the commensurate increase in birefringence because of structural reorganisation of the bilayer having taken place.

The differences here can be related to thermodynamic phases of the bilayers. For saturated bilayers in the gel phase, the lipid molecules are tightly packed into a configuration and cannot easily reorganise. Because of this, binding and penetration of peptides does not cause a single-phase permanent rearrangement of the bilayer, indicating that when some of the peptide is washed off during the dissociation phase, the bilayer recovers its organised structure. For unsaturated bilayers in the fluid phase, the lipid molecules are free to move and reorganise the membrane structure. Thus, when the peptide binds, the lipid molecules initially react as they did in the saturated bilayers (represented by section **H1** in Fig. 5b), but above a certain threshold of membrane-bound peptide mass and/or a threshold of membrane disorder, the unsaturated lipid molecules rearrange into a new structure. This change in structure is reflected in segment **H2** with its higher gradient. The dissociation phases **H3** and **L2** do not retrace the binding phase, confirming that an irreversible change in structure has occurred. These changes occur in the unsaturated bilayers only, demonstrating how the physical properties of the bilayer significantly affect the binding of the peptide and also the response of the bilayer to the peptide interaction. The turn downwards (lower birefringence) at the end of **H3** may correspond to entrapment of the peptide between the chip surface and the bilayer as a result of translocation through the membrane. Because the supported nature of the bilayer in this study prevents complete translocation of peptide, penetration and passage of the peptide to the inner membrane layer can therefore prevent reorganisation of the bilayer structure.

While these results show in some detail the changes in the bilayer, they do not point strongly towards any particular penetration mechanism. Previous results for HPA3 suggest that its mechanism for action proceeds through the formation of pores in the membrane (Park et al. 2008), however it is possible that other mechanisms may be involved. If pore formation does indeed occur, the permanent change in birefringence would suggest that the toroidal pore model is more likely than the barrel–stave model, because the barrel–stave model does not involve permanent reorganisation of the membrane whereas the toroidal pore model requires rotation of lipid molecules adjacent to the pores. Additionally, while it has been suggested that the carpet model is unlikely to explain peptide internalisation, because membrane integrity is maintained, it is possible that some peptides may briefly disrupt the membrane while traversing the bilayer, but leave the membrane in a state that allows it to reform and maintain its integrity. The results demonstrate, therefore, that the mechanism of HPA3 membrane binding involves a continuous change in bilayer structure from disruption to reorganisation which depends on the initial bilayer structure and peptide concentration.

Conclusions

The results of this study have demonstrated that the degree of bilayer order strongly affects the binding of membrane-interacting peptides and the changes in the bilayer during the binding process. In general, HPA3 was found to bind to all bilayers, although it bound more to the negatively charged lipid combinations DMPC–DMPG and POPC–POPG. However, the effect of HPA3 binding on the bilayer structure was found to be very different for unsaturated lipids than for saturated lipids, particularly in the dissociation phase. Dissociation of HPA3 from saturated lipids involved partial reversal of the binding phase whereas for unsaturated lipids the dissociation deviated significantly from the binding phase, indicating irreversible reorganisation of the membrane structure. This more complex behaviour reveals the biphasic nature of HPA3-induced changes in membrane which are not readily identified by other biophysical techniques and provides the basis for more detailed understanding of peptide–membrane interactions.

Acknowledgments We would like to thank the Faculty of Medicine Nursing & Health Sciences, Monash University and ATA Scientific for seed funding. The financial support of the Australian Research Council, the Potter Foundation and the European Union Framework 7 project ASMENA is also gratefully acknowledged.

References

Benes M, Billy D, Benda A, Speijer H, Hof M, Hermens WT (2004) Surface-dependent transitions during self-assembly of phospholipid membranes on mica, silica, and glass. Langmuir 20:10129–10137

Chen YH, Yang JT, Chau KH (1974) Determination of the helix and beta form of proteins in aqueous solution by circular dichroism. Biochemistry 13:3350–3359

Feijter F de, Benjamins J, Veer F (1978) Ellipsometry as a tool to study the adsorption behaviour of synthetic and biopolymers at the air-water interface. Biopolymers 17:1759–1772

Gehman JD, Luc F, Hall K, Lee TH, Boland MP, Pukala TL, Bowie JH, Aguilar MI, Separovic F (2008) Effect of antimicrobial peptides from Australian tree frogs on anionic phospholipid membranes. Biochemistry 47:8557–8565

Hall K, Mozsolits H, Aguilar M (2003) Surface plasmon resonance analysis of antimicrobial peptide-membrane interactions: affinity and mechanism of action. Lett Peptide Sci 10:475–485

Horvath R, Ramsden J (2007) Quasi-isotropic analysis of anisotropic thin films on optical waveguides. Langmuir 23:9330–9334

Jin Y, Mozsolits H, Hammer J, Zmuda E, Zhu F, Zhang Y, Aguilar MI, Blazyk J (2003) Influence of tryptophan on lipid binding of linear amphipathic cationic antimicrobial peptides. Biochemistry 42:9395–9405

Lee KH, Lee DG, Park Y, Kang DI, Shin SY, Hahm KS, Kim Y (2006) Interactions between the plasma membrane and the antimicrobial peptide HP (2–20) and its analogues derived from Helicobacter pylori. Biochem J 394:105–114

Lee T, Hall K, Swann M, Popplewell J, Unabia S, Park Y, Hahm K, Aguilar M (2010a) The membrane insertion of helical antimicrobial peptides from the N-terminus of *Helicobacter pylori* ribosomal protein L1. Biochim Biophys Acta 1798:544–557

Lee TH, Heng C, Swann MJ, Gehman JD, Separovic F, Aguilar MI (2010b) Real-time quantitative analysis of lipid disordering by aurein 1.2 during membrane adsorption, destabilisation and lysis. Biochim Biophys Acta 1798:1977–1986

Mashaghi A, Swann M, Textor JPM, Reimhult E (2008) Optical anisotropy of supported lipid structures probed by waveguide spectroscopy and its application to study of supported lipid bilayer formation kinetics. Anal Chem 80:3666–3676

Melo MN, Ferre R, Castanho MA (2009) Antimicrobial peptides: linking partition, activity and high membrane-bound concentrations. Nat Rev Microbiol 7:245–250

Mereuta L, Luchian T, Park Y, Hahm K (2009) The role played by lipids unsaturation upon the membrane interaction of the Helicobacter pylori HP(2-0) antimicrobial peptide analogue HPA3. J Bioenerg Biomembr 41:79–84

Mozsolits H, Aguilar MI (2002) Surface plasmon resonance spectroscopy: an emerging tool for the study of peptide-membrane interactions. Biopolymers 66:3–18

Mozsolits H, Wirth HJ, Werkmeister J, Aguilar MI (2001) Analysis of antimicrobial peptide interactions with hybrid bilayer membrane systems using surface plasmon resonance. Biochim Biophys Acta 1512:64–76

Papo N, Shai Y (2003) Exploring peptide membrane interaction using surface plasmon resonance: differentiation between pore formation versus membrane disruption by lytic peptides. Biochemistry 42:458–466

Park S, Kim M, Hossain M, Shin S, Kim Y, Stella L, Wade J, Park Y, Hahm K (2008) Amphipathic alpha-helical peptide, HP (2-20), and its analogues derived from Helicobacter pylori: pore formation mechanism in various lipid compositions. Biochim Biophys Acta 1778:229–241

Popplewell JF, Swann MJ, Freeman NJ, McDonnell C, Ford RC (2007) Quantifying the effects of melittin on liposomes. Biochim Biophys Acta 1768:13–20

Shai Y (2002) Mode of action of membrane active antimicrobial peptides. Biopolymers 66:236–248

Swann MJ, Peel LL, Carrington S, Freeman NJ (2004) Dual-polarization interferometry: an analytical technique to measure changes in protein structure in real time, to determine the stoichiometry of binding events, and to differentiate between specific and nonspecific interactions. Anal Biochem 329:190–198

Yu L, Guo L, Ding JL, Ho B, Feng SS, Popplewell J, Swann M, Wohland T (2009) Interaction of an artificial antimicrobial peptide with lipid membranes. Biochim Biophys Acta 1788:333–344

Zasloff M (2002) Antimicrobial peptides of multicellular organisms. Nature 415:389–395

Zwang TJ, Fletcher WR, Lane TJ, Johal MS (2010) Quantification of the layer of hydration of a supported lipid bilayer. Langmuir 26:4598–4601